Review Article

Pulmonary arteries: imaging of pulmonary embolism and beyond

Ellen M. Leitman[1], Shaunagh McDermott[2]

[1]Harvard Medical School, Boston, Massachusetts, USA; [2]Division of Thoracic Imaging and Intervention, Massachusetts General Hospital, Boston, Massachusetts, USA

Contributions: (I) Conception and design: All authors; (II) Administrative support: None; (III) Provision of study materials or patients: None; (IV) Collection and assembly of data: None; (V) Data analysis and interpretation: None; (VI) Manuscript writing: All authors; (VII) Final approval of manuscript: All authors.

Correspondence to: Shaunagh McDermott. Massachusetts General Hospital, Boston, Massachusetts, USA. Email: mcdermott.shaunagh@mgh.harvard.edu.

Abstract: The pulmonary arteries are not just affected by thrombus. Various acquired and congenital conditions can also affect the pulmonary arteries. In this review we discuss cross sectional imaging modalities utilized for the imaging of the pulmonary arteries. Acquired pulmonary artery entities, including pulmonary artery sarcoma (PAS), vasculitis, aneurysm, and arteriovenous malformations, and congenital anomalies in adults, including proximal interruption of the pulmonary artery, pulmonary sling, pulmonary artery stenosis, and idiopathic dilatation of the pulmonary trunk, are also discussed. An awareness of these entities and their imaging findings is important for radiologists interpreting chest imaging.

Keywords: Computed tomography (CT); pulmonary embolus (PE); pulmonary artery sarcoma (PAS); pulmonary artery aneurysm; pulmonary arteriovenous malformation; congenital anomalies

Submitted Jun 03, 2018. Accepted for publication Aug 13, 2018.
doi: 10.21037/cdt.2018.08.05
View this article at: http://dx.doi.org/10.21037/cdt.2018.08.05

Introduction

A pulmonary artery anomaly can be suspected based on clinical findings or chest radiographic findings, or can be incidentally detected on cross-sectional imaging. In this article we briefly discuss the cross-sectional imaging modalities utilized in the evaluation of the pulmonary arteries, followed by a review of the imaging features of various acquired and congenital entities of the pulmonary arteries, with an emphasis on their computed tomography (CT) appearances.

Imaging modalities

CT pulmonary angiography (CTPA)

CTPA was introduced in 1992 (1) and since then it has become the diagnostic test of choice in patients with suspected pulmonary embolus (PE). Adequate contrast opacification of the pulmonary vasculature is necessary to demonstrate intravascular filling defects. Vessel opacification depends on both patient factors such as weight and cardiac output, and imaging protocol factors including volume of contrast injected and rate and duration of injection (2,3). Ideally the contrast attenuation of the pulmonary arteries for diagnostic purposes is equal to or greater than 250 HU.

Fixed scan delay for initiating scanning should not be used as it does not consider the variations in cardiac functions. There are two techniques used to determine the scan delay after contrast injection: (I) test bolus injection; and (II) automated bolus tracking. For both techniques, a pre-monitoring, non-contrast axial image is acquired at the level of the main pulmonary trunk. In the test bolus technique, a small amount of contrast (10–20 mL) is injected and after a delay of 5–10 seconds a series of low radiation dose axial images (100–120 kV, 10–20 mAs) are acquired at the level of the main pulmonary trunk at 1–2 second intervals. A region of interest (ROI) is drawn on the main pulmonary trunk or right ventricle, from which an enhancement curve is generated. From this curve the time needed to reach the peak contrast enhancement is calculated. Two to six seconds are added to this to allow the bolus to establish a more uniform plateau throughout the pulmonary arteries. Shorter delay is appropriate for

longer scan duration (≥5 seconds) and longer delay allows better enhancement for faster scanners (<5 seconds). A second contrast injection is then administered for CTPA. For automated bolus tracking, ROI is drawn on the main pulmonary trunk or right ventricle in the pre-monitoring image and a series of axial low-dose monitoring scans are acquired every 1–2 seconds, starting 5–10 seconds after the start of the contrast injection. The scan is initiated when a predetermined threshold (usually +100 HU above the baseline) is reached plus 4–6 second delay. The delay accounts for table movement to start scan location, breathing instruction and switch of scanning mode from the axial to the helical scanning mode.

The rate of injection is important for obtaining homogeneous enhancement and adequate opacification of smaller vessels. Typically, a flow rates of 4–5 mL/s are suggested for CTPA (4). CTPA at lower tube potential (≤100 kV) or dual energy scanning mode in average to small size patients can be performed at contrast injection rates of 2–4 mL/s. The duration of injection affects the peak time of contrast enhancement and the magnitude of contrast enhancement. Regarding contrast volume, a larger volume results in greater and longer enhancement which is dependent on patient body weight. Recently, there is a trend towards weight-tailored volume of contrast material. The iodine concentration of the agent is also important. The use of high iodine concentration agents (i.e., 350, 370, or 400 mg/mL) allows a lower volume of contrast and the injection rate to be decreased. However, when using these high iodine concentration agents, it is ideal to use a biphasic injection protocol with a saline flush immediately after the contrast material to decrease perivenous streak artifact at the level of the brachiocephalic vein (3). At our institution, patients receive 65–80 mL of intravenous iodinated contrast (iopamidol 370 mgI/mL, Bracco Diagnostics, Princeton, NJ, USA), based on the patient's weight (≤70 kg: 65 mL and >70 kg: 80 mL), injected at 4 mL/seconds. With low tube potential or dual energy scanning modes, lower contrast concentration (or with dilution of contrast with saline) and smaller contrast volumes are often sufficient to obtain optimal contrast enhancement unless the patients have large body habitus. For patients who cannot receive typical amount of contrast media due to renal dysfunction or recent contrast injection for any procedure (<24 hours), we use 25 mL (<70 kg) or 35 mL (70–90 kg) of contrast volume (370 mgI/mL) with dual energy scanning mode.

Appropriate breath holding is quintessential for optimal CTPA. Patients are instructed to avoid taking deep breaths before holding their breath in order to avoid transient interruption of contrast inflowing from the superior vena cava by the unopacified blood from the inferior vena cava. Bolus interruption is a frequent cause of suboptimal contrast enhancement in CTPA study. To overcome this limitation, some centers recommend no breath hold for CTPA with high-speed scanning (scan time <1 second for the entire chest). On the newer scanners with <5 second scan time, scanning direction (craniocaudal or caudocranial direction) has no difference in contrast related artifacts or enhancement of pulmonary arteries.

Dual-energy CT (DECT) refers to the near-simultaneous acquisition of CT images at two different X-ray energy levels. Imaging at both high and low kilovoltages results in the combination of greater photoelectric absorption afforded by low voltage and lower image noise afforded by high voltage. Low kilovoltage monochromatic images (<60 keV) can (I) increase the enhancement of the pulmonary arteries when enhancement is suboptimal on single-energy images; and (II) provide optimal diagnostic enhancement of the pulmonary arteries using a reduced volume of iodinated contrast (5). Post-processing of DECT data sets allows the generation of material decomposition images, including virtual unenhanced (VNC) images and blood volume images. Blood volume images allows quantification of iodine distribution and lung perfusion.

Magnetic resonance imaging (MRI)

MRI may become an attractive alternative to CTPA for the diagnosis of PE, with the advantage of no ionizing radiation, and possible reduced risk of complications from contrast administration, particularly if newer nonenhanced MR sequences are used. There are, however, some disadvantages to MRI that have thus far prevented it from being widely adopted for the evaluation of PE. These include significant longer acquisition time and lower spatial resolution compared to CT. In acutely ill and unstable patients, MRI can be challenging because of the longer breath-holds and examination times, and also the requirement of dedicated MRI-compatible monitoring devices. Another possible disadvantage of MRI is the risk of missing a pertinent alternative diagnosis. Also, the relative lack of familiarity with MR angiography (MRA) for evaluation of PE may contribute to technical inconsistency, the primary reason for the underperformance of MRA for the detection of subsegmental emboli in the PIOPED III study (6).

MR techniques used for evaluating the pulmonary arteries

include MRA with and without contrast enhancement, MR perfusion imaging, and more novel MRI techniques. Contrast enhanced MRA (ce-MRA) consists of a heavily T1-weighted gradient-echo sequence; a short TR is used to allow a short breath hold, and a short TE to decrease background noise. There are two different approaches for ce-MRA. The first is to acquire 3D volume data of the pulmonary vasculature with high spatial resolution, ideally with isotropic spatial resolution in all directions. The utilization of parallel imaging allows the acquisition of sub-centimeter pulmonary ce-MRA in less the 20 seconds (7). The other approach is time resolved MRA, which achieves a high temporal resolution due to a multiphasic acquisition. The scan time can be as low as 5 seconds which makes this technique useful in dyspneic patients. Other advantages include better separation of contrast between veins and arteries (8), and it is less sensitive to incorrect bolus timing.

Regarding non-contrast-enhanced MRA sequences, steady-state free precession (SSFP) is a free-breathing real-time imaging technique which is useful for imaging patients who are not capable of a 5-second breath-hold (9). Navigator gating, a technique used to obtain images during the same phase of the respiratory cycle without the need for breath-hold, can be added to decrease motion or breathing artifacts in dyspneic patients. This technique exploits the differences between the relatively high T2/T1 ratio of blood compared to most other tissues. This inherent T2-contrast allows for differentiation of embolus from surrounding blood without the need for contrast (10).

In MR perfusion, a signal is generated based on the volume of blood in a region rather than directly imaging vascular structures. Perfusion imaging can be obtained after acquiring ce-MRA imaging, without the need for a further contrast injection. It is performed using a 3D fast low-angle shot (FLASH) gradient-echo sequence, and requires breath-holds during acquisition of images. Non-enhanced MRI lung perfusion imaging can also be performed. One option is to use a short echo-spacing half-Fourier fast spin-echo sequence to visualize pulsatile lung signal intensity changes during the cardiac cycle. Image subtraction between the systolic and diastolic phases allows the visualization of perfused lung tissue (11). Another nonenhanced technique is arterial spin labelling which utilizes blood water as an endogenous, freely diffusible tracer which can be exploited to detect signal change due to perfusion (12).

Other MRI techniques for imaging PE include direct thrombus imaging (DTI), and the use of fibrin-targeted contrast agents. DTI utilizes the presence of methemoglobin in a thrombus to allow it to be visualized without the need for contrast. It uses a T1-weighted sequence which exploits the T1-shortening due to methemoglobin in the thrombus, which results in a higher signal than in surrounding tissue (13). Fibrin-targeted contrast agents consists of gadolinium combined with a peptide that binds to fibrin within in the thrombus. Most of the studies on these agents are in animal models, with studies in humans ongoing (14).

An advantage of MRI is the ability to assess cardiac function during the same imaging session. Cine MRI can be used to quantify right ventricular (RV) ejection fraction. Cine MRI can also be used to assess cardiac motion and for the presence of pathologic changes such as bowing of the interventricular septum towards the left ventricle (15,16). Another noninvasive way to assess cardiac function is phase-contrast MRI flow measurements (17).

Fluorodeoxyglucose positron emission tomography (FDG-PET)

PET imaging with ^{18}F-FDG, a glucose analogue, shows increased tracer uptake in metabolically active processes. It is often performed in the evaluation and staging of malignancy, but increased FDG avidity is also seen in inflammatory and infectious processes (18). With respect to the pulmonary arteries, PET and PET-CT has a role to play in (I) identifying if a pulmonary artery lesion as malignant if it demonstrates high FDG avidity; and (II) identifying active vasculitis and monitoring response to treatment.

Acquired pulmonary artery entities

Pulmonary thromboembolism

PE is a serious condition, which is responsible for significant morbidity and mortality. PE is the third leading cause of death from cardiovascular conditions after coronary artery disease and cerebrovascular accident (19).

Although imaging has a key role in the diagnosis of PE, clinical assessment of the patient is the first and most crucial step. Clinical signs of PE are non-specific and can range from asymptomatic state and spontaneous resolution to dyspnea, pleuritic chest pain, tachypnea, tachycardia and hemoptysis to shock and death. When a PE is suspected, the clinical probability of PE should be determined before proceeding with testing (20). Validated scoring systems include, but is not inclusive of, the Modified Wells Scoring System (21), the Revised Geneva Scoring System (22), and the Pulmonary

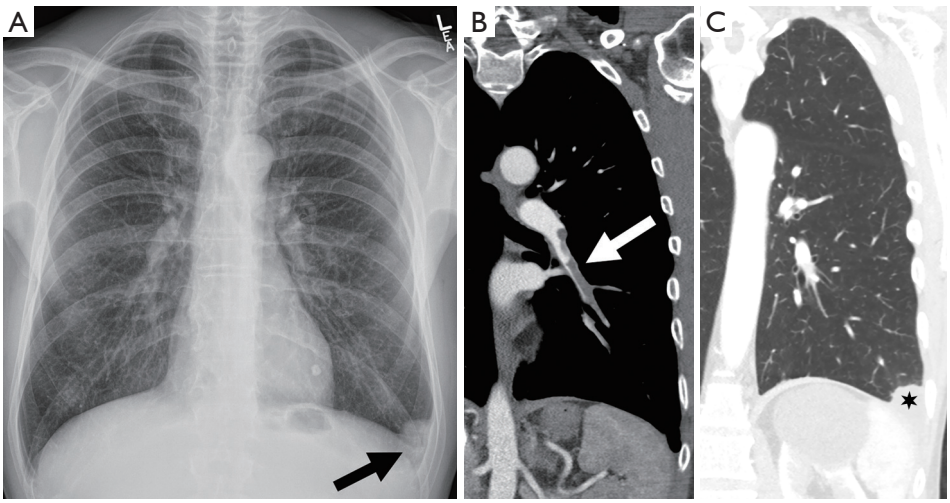

Figure 1 Pulmonary infarct and Hampton's hump. (A) Frontal chest radiograph demonstrating a wedge-shaped opacity in the left lower lung near the costophrenic sulcus (arrow), abutting the pleura (Hampton's hump). (B) Coronal CT image on mediastinal windows demonstrates a filling defect in the left lower lobe pulmonary artery (arrow). (C) Coronal CT image on lung windows shows a wedge-shaped area of consolidation abutting the pleura (star) consistent with an infarct.

Embolism Rule Out Criteria (PERC) (23). Recent guidelines have suggested that in patients who have a low pretest probability of PE and who meet all Pulmonary Embolism Rule Out Criteria, D-dimer measurements or imaging should not be obtained; in patients who have an intermediate pretest probability of PE or in patients with low pretest probability of PE who do not meet all Pulmonary Embolism Rule Out Criteria, a D-dimer measurement should be obtained as the initial diagnostic test, with imaging only considered if positive; and in patients with high pretest probability of PE CTPA should be obtained (24). D-dimer testing should not be used when the clinical probability of PE is high as the test has low negative predictive value in such cases (25).

One study found that after the implementation of a computerized decision support system, the rate of positive PE diagnosis on CTPA increased from 8.3% to 12.7%, and would have been even higher (16.7%) if the emergency physicians had adhered to the outcome of the decision support system in all cases (26). When pretest clinical decision support is used, CTPA has been shown to be highly sensitive and specific. However, it is surprisingly inaccurate in patients with low pretest probability, with a reported false-positive rate of 42% in the PIOPED II trial (27).

Imaging of PE

Chest radiography

Radiographic abnormalities in patients with acute PE, although very common, are nonspecific. A chest radiograph is obtained to exclude other diagnoses that might mimic a PE, such as pneumonia, pneumothorax, or rib fracture, and to provide information to help interpret the scintigram.

Radiographic signs that have been described in patients with acute PE include oligemia of the lung beyond the occluded vessel (Westermark sign), a large central pulmonary artery due to central thrombus (Fleischner sign) with abrupt tapering of the occluded pulmonary artery distally creating the 'knuckle sign', or an infarct presenting as peripheral wedge-shaped consolidation abutting the pleura (Hampton's hump) (*Figure 1*). However, Prospective Investigation of Pulmonary Embolism Diagnosis (PIOPED) demonstrated that these radiographic signs do not provide sufficient information to accurately establish or exclude the diagnosis of PE (28).

Ventilation/perfusion scintigraphy

This study relies on indirect signs for the diagnosis of PE. Xenon 133 or technetium 99m (Tc-99m) diethylenetriamine-pentaacetic acid are the usual inhaled ventilation agents, and Tc-99m macroaggregated human albumin is the perfusion agent that is injected intravenously. A diagnosis of a PE is made if the perfusion scan shows two or more wedge-shaped defects in a segmental or larger vascular distribution, and the absence of abnormal ventilation in the same lung segments (ventilation-perfusion mismatch) (*Figure 2*). When interpreting the scintigram, it is important to evaluate a

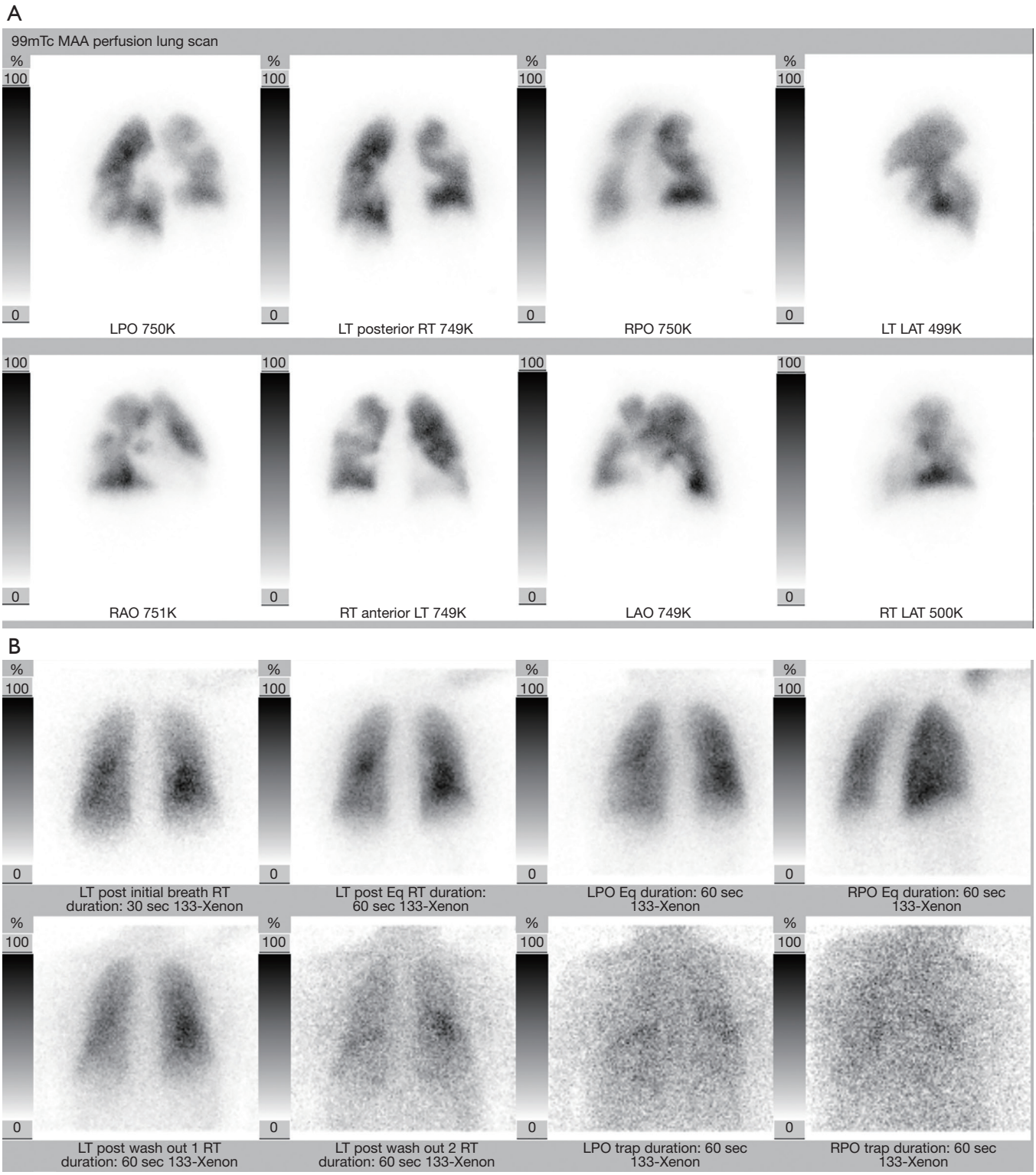

Figure 2 Acute pulmonary embolus on ventilation/perfusion scintigraphy. (A) Perfusion scan demonstrating bilateral moderate and large perfusion defects. (B) Ventilation scan demonstrating normal ventilation. Findings are consistent with high probability of PE. PE, pulmonary embolus.

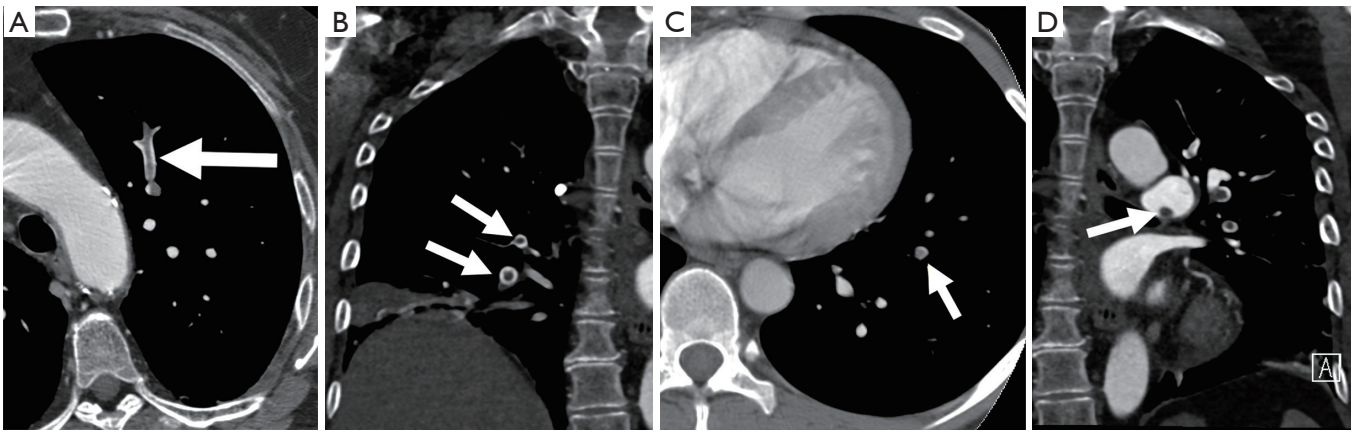

Figure 3 CT findings of acute pulmonary embolus. (A) There is a central filling defect surrounded by contrast within a left upper lobe segmental pulmonary artery (arrow) (railway track sign). (B) There are central fillings defects surrounded by contrast (polo mint sign) in right middle lobe segmental arteries (arrows). (C) There is a filling defect in a left lower lobe subsegmental artery (arrow), which is distended compared to adjacent arteries. (D) There is an eccentric filling defect in the left main pulmonary artery (arrow) which forms an acute angle with the pulmonary arterial wall.

current chest radiograph.

Based on the PIOPED II criteria, V/Q scans are reported according to the likelihood of a PE being present as one of the following: normal, very low probability for PE (<10%), low probability for PE (10–19%), intermediate-probability for PE (20–79%), or high probability for PE (>80%) (29). A more recent study found that perfusion scintigraphy combined with chest radiography can provide diagnostic accuracy similar to both CTPA and ventilation-perfusion scintigraphy, at lower cost and with lower radiation dose (30).

CT

The ultimate goal of CTPA is to provide high contrast opacification of the pulmonary arteries, using the lowest possible volume of contrast material, minimizing radiation dose and shortening the acquisition time while maintaining adequate image quality.

Acute PE: typically, findings of an acute PE on contrast-enhanced CTPA are complete or partial filling defects in the pulmonary arteries. Partial filling defects can be centrally or peripherally located within the artery and will be surrounded by contrast. Centrally located defects can be detected as the 'polo mint sign' on transverse images and the 'railway track' on longitudinal images (1,31). Peripherally located filling defects make an acute angle with the arterial wall (1,32). The occluded artery may be enlarged compared to the patent vessels nearby (31) (*Figure 3*). Respiratory motion, image noise, flow-related artifacts, or streak or beam-hardening artifact may result in the misdiagnosis of PE. A false diagnosis of PE can also be made if a poorly opacified pulmonary vein or a mucus plugged bronchus is inadvertently identified as a pulmonary artery. A study found that pulmonary emboli diagnosed on CTPA were frequently over-diagnosed (26% of cases) when compared with the consensus opinion of a panel of expert chest radiologists; with discordance occurring more often when the original reported PE was solitary (46% of reported solitary PEs were considered negative on retrospective review) and located in a segmental or subsegmental pulmonary artery (27% of segmental and 59% of subsegmental PE diagnoses were considered negative on retrospective review) (33).

Pulmonary infarcts can be seen in association with acute PE. They are often wedge-shaped, based at the pleura with apexes directed toward the hilum and exhibit lower lobe predominance (34). They may appear as consolidation, ground glass opacity or as an area of ground glass opacification surrounded by a rim of consolidation ('reversed halo' sign) (35). A recent study reported that a single 'reversed halo' sign with low-attenuation area inside the rim with or without reticulation and with peripheral lower lobe predominance is highly suggestive of pulmonary infarct specifically due to PE (36). As an infarct resolves, it decreases in size from the periphery (the 'melting sign') and becomes more nodular (34).

DECT pulmonary angiography provides several

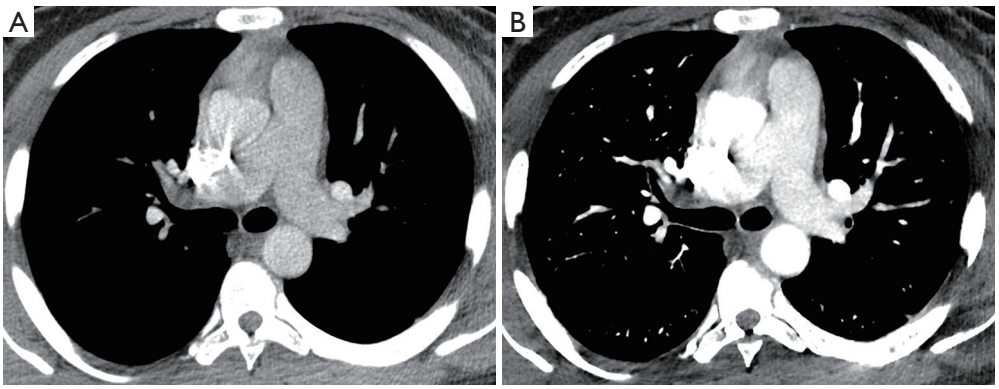

Figure 4 Dual-energy CT. (A) Axial blended CT image in which the attenuation of the main pulmonary artery measures 128 HU. (B) Corresponding axial virtual monochromatic CT image at 40 keV in which the attenuation of the main pulmonary artery measures 400 HU.

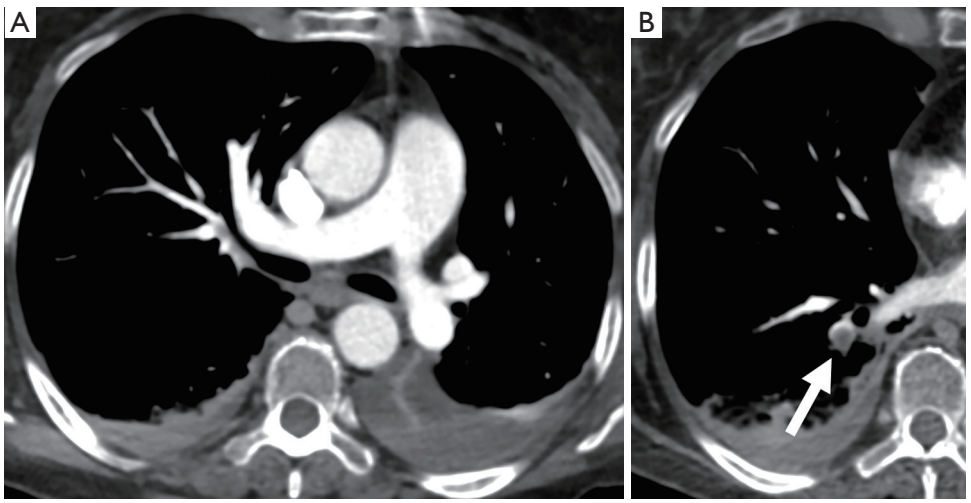

Figure 5 Dual-energy CT using reduced volume of iodinated contrast. (A) Axial virtual monochromatic CT image at 40 keV shows optimal opacification of the pulmonary arteries (main pulmonary artery measures 711 HU). (B) There is a filling defect in a right lower lobe segmental artery (arrow).

potential advantages over single-energy scans, as described above. The ability to reconstruct virtual low-energy monochromatic images can increase the enhancement of the pulmonary arteries (37) and may salvage a CTPA study which would be considered nondiagnostic due to suboptimal arterial enhancement on a single-energy scanner (*Figure 4*). Low virtual monochromatic images may also provide optimal, diagnostic enhancement of the pulmonary arteries with a reduced volume of contrast material (*Figure 5*) (38). In addition to anatomic images, material decomposition images, such as iodine maps and pulmonary blood volume (PBV) images, are obtained and provide additional information about pulmonary perfusion. In some cases of PE without infraction, there are areas of decreased attenuation on PBV images, with no corresponding opacity on CT images obtained with lung windows (5) (*Figure 6*). In cases of infarct, there is a peripheral wedge-shaped area of nonenhancement that can be larger than the opacity seen on images obtained with lung windows (*Figure 7*).

There is growing evidence that CTPA also plays a role in the assessment of PE severity and prognosis, possibly being even superior to PE severity index (PESI), which is the main prognostic prediction rule for PE based on clinical information (39). Classically, RV enlargement, defined as the ratio of RV dimension to left ventricular (LV) dimension greater than 0.9, on reconstructed CT four-chamber view

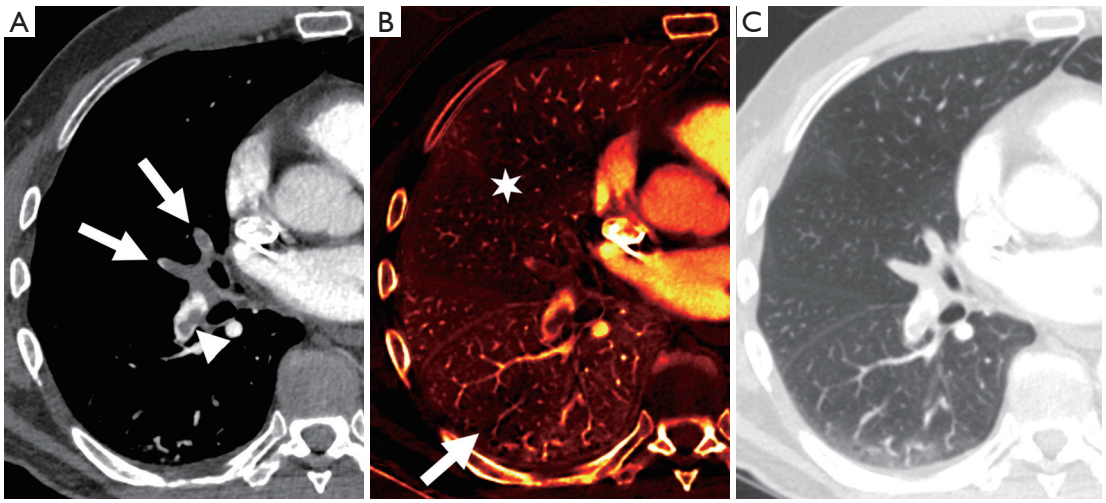

Figure 6 Pulmonary embolism on dual-energy CT. (A) Axial CT image on mediastinal windows demonstrates complete occlusion of segmental right middle lobe pulmonary arteries (arrows) and an eccentric filling defect in the right lower lobe pulmonary artery (arrowhead). (B) Pulmonary blood volume image demonstrates decreased perfusion of the right middle lobe (star) and right lower lobe (arrow) compared to the remainder of the lungs. (C) There is no corresponding abnormality of the lung parenchyma on lung windows.

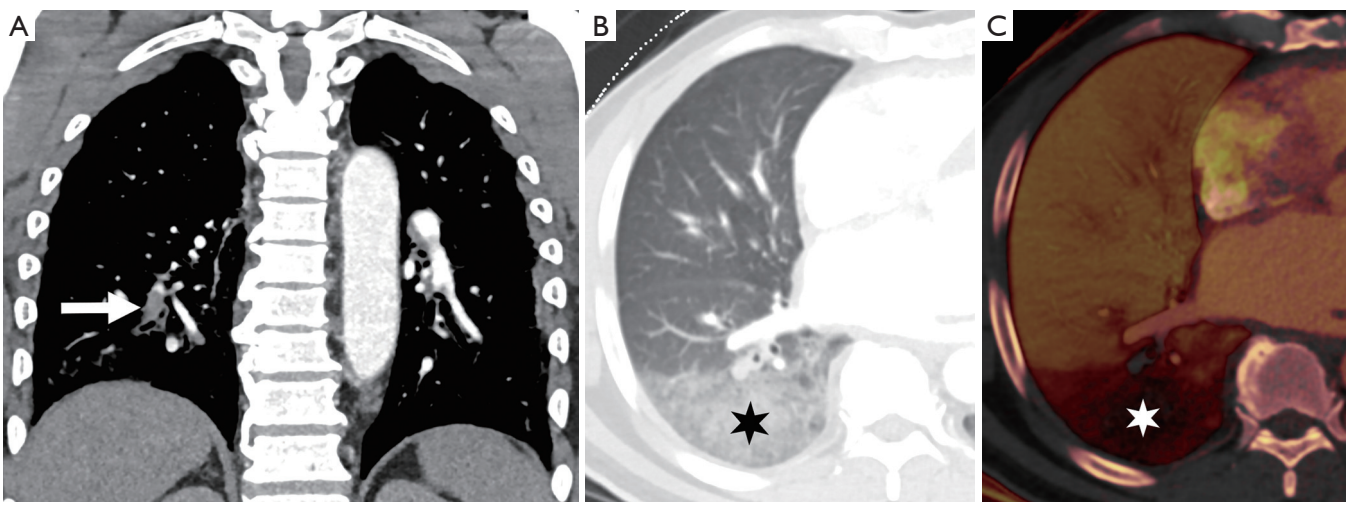

Figure 7 Pulmonary embolism and infarct on dual-energy CT. (A) Coronal CT shows complete occlusion of a right lower lobe segmental artery (arrow). (B) Axial CT image on lung windows demonstrates a mixed-attenuation opacity in the right lower lobe (star). (C) Pulmonary blood volume image demonstrates decreased perfusion in the right lower lobe (star).

correlates with RV dysfunction on the echocardiogram (40,41) and helps predict 30-day death, even after adjusting for pneumonia, cancer, chronic lung disease and age (42). Generating the four-chamber view requires a workstation capable of 3D postprocessing, additional time and expertise compared to measuring the RV/LV ratio on axial imaging. Studies have shown that there is no statistical significant difference between four-chamber and axial measurements (43,44), and in predicting 30-day mortality after acute PE (45). To calculate the right ventricle/left ventricle ratio, the ventricular chambers are measured in the axial plane at their widest points between the inner surface of the free wall and the surface of the interventricular septum, which may be at slightly different axial images (*Figure 8*). In a meta-analysis of 49 studies with >13,000 patients, an abnormal increase of RV/LV diameter ratio was found to

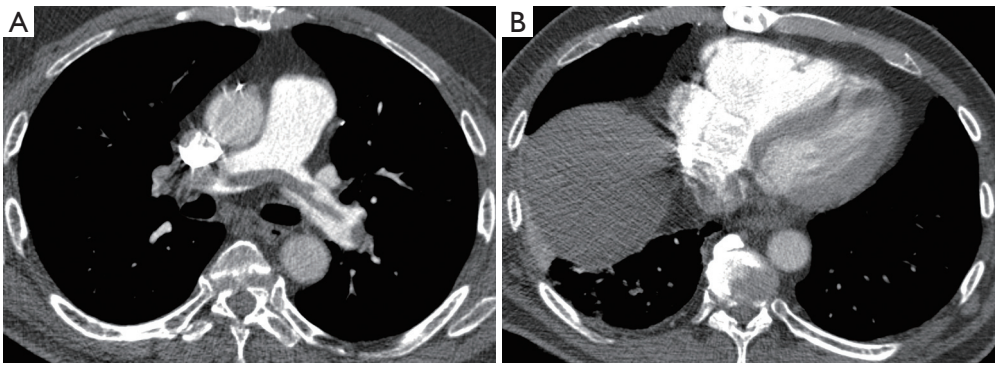

Figure 8 Saddle embolus and right heart strain. (A) Axial image depicts a saddle embolus. (B) Axial image through the heart shows a right ventricle/left ventricle ratio greater than 1, which is consistent with right heart strain.

have the strongest predictive value for adverse outcome, all-cause mortality and PE-related mortality when compared to thrombus load and central location (46).

Other imaging markers of right heart strain include reflux of contrast into the hepatic veins, dilated main pulmonary artery, and straightening or leftward bowing of the interventricular septum. Recent studies have suggested that PE attenuation (47), and the time it takes for contrast to reach a predefined threshold in a ROI in the pulmonary trunk ('time to threshold') (48) may be potential imaging biomarkers. Dual energy CTPA may also have a prognostic role in patients with PE. The overall extent of PBV defects has been shown to correlate with RV strain determined by RV/LV ratios, and endoluminal clot burden (49-52).

Clot burden assessments, such as the Mastora and Qanadli scores, are cumbersome and not routinely used in clinical practice. One study found no correlation between the obstruction index and all-cause death or clinical deterioration in 448 patients, however in the subgroup of hemodynamically stable patients, central emboli were associated with an increased risk or all-cause death or clinical deterioration (53). Furthermore, a meta-analysis found no correlation between obstruction index (according to the Qanadli scoring system) and 30-day mortality but that localization of emboli can be used for risk stratification (54).

Chronic PE: most pulmonary emboli resolve without sequelae. However, in a small percentage of patients, particularly those with large or recurrent emboli, the thrombi may not completely resolve. CT findings of a chronic PE include (I) complete occlusion of a vessel; (II) lines of decreased opacity that traverse the lumen of contrast-filled pulmonary arteries known as webs or bands; (III) scalloped look of arterial walls that reflects intimal irregularity; (IV) abrupt narrowing of the major pulmonary vessels; (V) eccentrically located crescent-shaped filling defects that form obtuse angles with the vessel wall; (VI) contrast flowing through thickened pulmonary arteries due to recanalization; (VII) calcification of the filling defect (55-57) (*Figure 9*). Another feature that can help distinguish between acute and chronic thrombi is that vessels in acute PE are expanded due to pulsatile flow, while in chronic emboli vessels are markedly attenuated distal to the obstruction (58). Secondary signs of chronic pulmonary emboli include abnormal enlargement of bronchial and systemic collateral vessels, mosaic attenuation of the lung parenchyma, enlargement of the main pulmonary artery diameter, and peripheral pleura-based wedge-shaped densities which represent old infarcts (31,59-63). The differential diagnosis of chronic thromboembolus and differentiating CT features are outlined in *Figure 10*.

MRI

On MRA the imaging features are similar to those on CTPA (*Figure 11*), except in cases of a completely occlusive emboli which can appear as an abrupt vessel cut-off on MRA. This may make the identification of occlusive emboli more difficult on MRA than on CTPA because an absent vessel may be more challenging to identify. Truncation artifact can rarely cause an apparent central hypointensity in a pulmonary artery. However, this can be differentiated from a PE by using a signal drop cutoff of 50%; if the signal decreases by more than 50% the central hypointensity is likely a PE (64).

On SSFP images the pulmonary vessels are bright, with the embolus being low signal intensity (65). On MR perfusion images, areas of decreased or absent blood flow suggests the presence of an obstruction, thereby indirectly

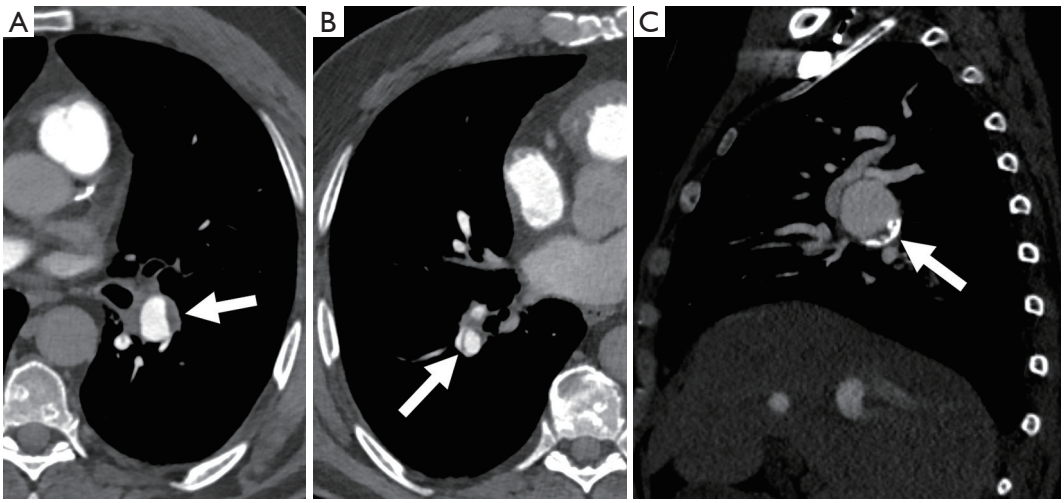

Figure 9 CT findings of chronic pulmonary embolus. (A) There is a peripheral filling defect in a left lower lobe pulmonary artery which forms an obtuse angle with the pulmonary artery wall (arrow). (B) There is a web within a contrast filled right lower lobe pulmonary artery (arrow). (C) There is a peripheral filling defect in the right main pulmonary artery which is calcified (arrow).

demonstrating a PE (66).

Non-thrombotic PE

Non-thrombotic PE is an uncommon condition. It usually involves particles that are so small that they are not depicted as intra-arterial filling defects. Possible etiologies include droplets of fat, bubbles of air or nitrogen, tumors, and foreign bodies such as talc or cement (67).

Pulmonary artery sarcoma (PAS)

PAS is a rare malignancy that originates from pluripotent cells in the pulmonary artery intima. It predominantly affects the pulmonary trunk and bilateral main pulmonary arteries, but can involve the pulmonary valve and RV outflow track, and rapidly metastasize to the lungs (68,69). Clinical symptoms are non-specific and similar to those of chronic thromboembolic disease—dyspnea, tachypnea, palpitations, chest pain, syncope, fever, and hemoptysis—which results in overwhelming misdiagnosis of PAS as chronic thromboembolic disease (70-73). Radical resection with chemotherapy and radiotherapy is the treatment of choice but even with the appropriate treatment the prognosis is very poor, with a median survival estimated at 24.7±8.5 months for patients with multimodality treatment and 8±1.7 months for patients with single modality treatment (69). Therefore, early diagnosis is critical to an optimal prognosis.

As with clinical presentation, imaging findings are similar between PAS and PE and manifest as filling defects of the pulmonary vessels. However, imaging features that can help differentiate between the two conditions exist. One study reported that the filling defect in PAS is low-attenuating defect on CT that occupies the entire lumen of the proximal or main pulmonary artery and often extends extraluminally (74). The morphology of PAS and chronic pulmonary thromboembolism was recently compared on CT (75). PAS appeared as expansive lesions with widening of the corresponding pulmonary artery; the proximal end of the tumor was usually bulging and lobulated, while the distal end distended assuming an aneurysm- or grape-like appearance (75,76). In contrast, chronic thromboemboli were usually attached to the pulmonary artery intima and the proximal end was typically straight and cup-shaped (75). Unlike acute PE, both PAS and chronic thromboemboli can demonstrate post-contrast enhancement on CT; however, sarcoma is lobulated (*Figure 12*) and usually forms acute angles with vessel wall while chronic thromboemboli forms obtuse angles (31). Calcifications are more frequently found in chronic thromboembolus than in PAS (75) (*Figure 9*).

DECT angiography has also been proposed to be useful in detecting PAS, particularly in patients without predisposing factors for PE (77). Chang *et al.* measured iodine-related Hounsfield units and iodine concentration of the filling defect in the main pulmonary artery and found

Chronic pulmonary embolus	Acute pulmonary embolus
Decrease in pulmonary artery diameter	Increase in pulmonary artery diameter
Peripheral, crescent-shaped defect with obtuse angle with pulmonary artery wall	Eccentric filling defect with acute angle with pulmonary artery wall
Web or flap (linear filling defect)	
Calcification of the thrombus	
Dilatation of bronchial arteries is common	
Mosaic attenuation of the lungs	
Chronic pulmonary embolus	**Pulmonary artery sarcoma**
Filling defects may be complete or partial	Filling defect completely occludes the main or proximal pulmonary arteries, which may appear distended
Filling defects associated with decreased lumen diameter	Possible extension into the lung or the mediastinum
Filling defects remain intraluminal	Delayed enhancement on CT or MR
Absence of enhancement or FDG avidity	Increased FDG avidity
Chronic pulmonary embolus	**Pulmonary artery vasculitis**
Intraluminal filling defects	Concentric mural thickening of the pulmonary artery
No involvement of systemic arterial circulation	Possible involvement of the aorta and its branches
	Unilateral pulmonary artery occlusion can occur late in the disease
	Increased FDG avidity in active disease
Chronic pulmonary embolus	**Proximal interruption of the pulmonary artery**
Diagnosed in adulthood	More commonly diagnosed in childhood
Multiple bilateral arterial abnormalities	Single site of occlusion
Abrupt vascular tapering with intraluminal filling defects	Smooth tapering of pulmonary artery, which ends at the hilum, without endoluminal changes

Figure 10 CT features allowing differentiation of chronic pulmonary embolus from other obstructive disorders of the pulmonary artery.

these values to be significantly different between pulmonary thromboembolism and PAS (77). ^{18}F-FDG-PET may also have a role in differentiating between PAS and chronic thromboembolus, as some studies report FDG uptake by PAS (78) (*Figure 12*).

Recently, MRI was suggested to be particularly useful in differentiating between PAS and chronic thromboembolus (75,76). The pattern of MRI contrast enhancement of PAS was found to be cloudy with delayed inhomogeneous enhancement; time-signal intensity curves consistently showed a gradual rise type (75). In contrary, chronic thromboemboli did not demonstrate an obvious enhancement and the intensity curves showed a platform type (75). In another study Liu *et al.* further showed that the hyperintense filling defect in the main pulmonary artery on fat suppressed T2-weighted MRI was a specific sign of PAS, not seen in chronic thromboemboli (76).

Pulmonary artery vasculitis

Large-vessel vasculitides, such as Takayasu arteritis, giant cell arteritis (GCA) and Behçet disease, predominantly affect the aorta and its largest branches, however the pulmonary arteries can also be involved.

Takayasu arteritis

Takayasu arteritis is an idiopathic vascular disorder, characterized by granulomatous inflammation of the arterial wall with marked intimal proliferation and fibrosis of the

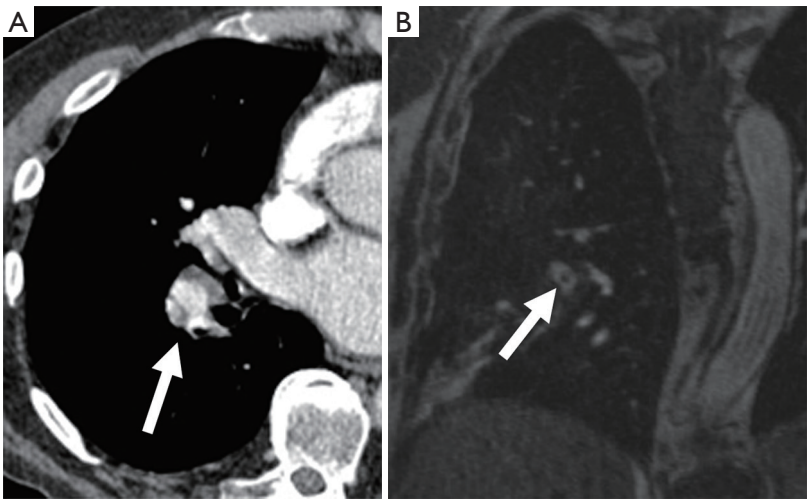

Figure 11 Chronic pulmonary embolus on CTPA and MRA. (A) Axial contrast-enhanced CT demonstrates a web within a contrast filled right lower lobe segmental pulmonary artery (arrow). (B) Coronal contrast-enhanced MRA in the same patient depicts the web in a right lower lobe segmental pulmonary artery (arrow). CTPA, CT pulmonary angiography; MRA, MR angiography.

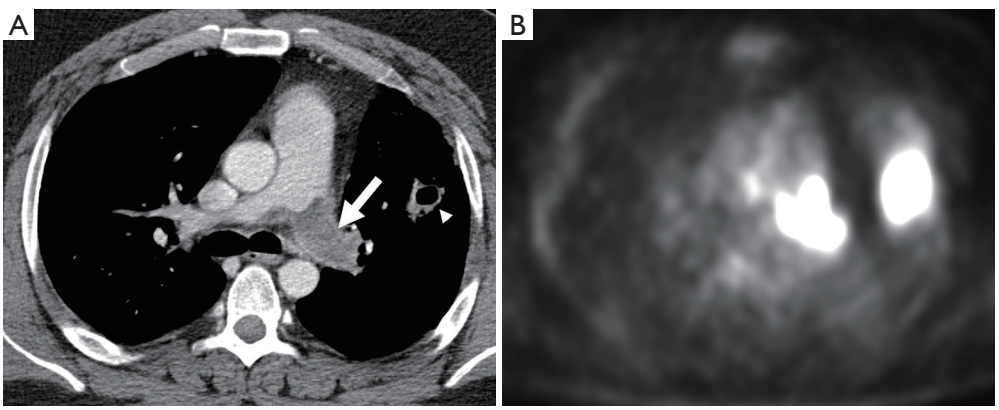

Figure 12 Pulmonary artery sarcoma. (A) Axial contrast-enhanced CT demonstrates a complete filling defect occluding the left main pulmonary artery (arrow) and a cavitary nodule in the left upper lobe (arrowhead). (B) Both the filling defect and the cavitary nodule demonstrate intense uptake on F18 FDG-PET. This was confirmed to be a pulmonary artery angiosarcoma on biopsy. The cavitary nodule represented a lung metastasis.

media and adventitia resulting in stenosis, and occlusion (79). Occasionally, poststenotic dilatations and aneurysms can develop when inflammation destroys the media. It affects almost exclusively patients less than 40 years of age. It can involve the throacoabdominal aorta and its branches, and the pulmonary arteries.

Pulmonary artery involvement occurs in 50–80% of patients, often being a late manifestation of the disease. A common finding is stenosis or occlusion of the segmental and subsegmental arteries, and less commonly of the lobar or main pulmonary arteries (80). CT manifestations of pulmonary artery involvement include wall thickening (*Figure 13*) and enhancement in the early phase of the disease, and luminal stenosis or occlusion and mural calcification in the chronic phase. Unilateral occlusion can occur in advanced disease, and Takayasu arteritis should be considered in cases of chronic pulmonary artery obstruction of unknown origin. Collaterals can develop in chronic cases depending on the site and severity of the stenosis.

MRI can also be used and is preferred over CT, in this

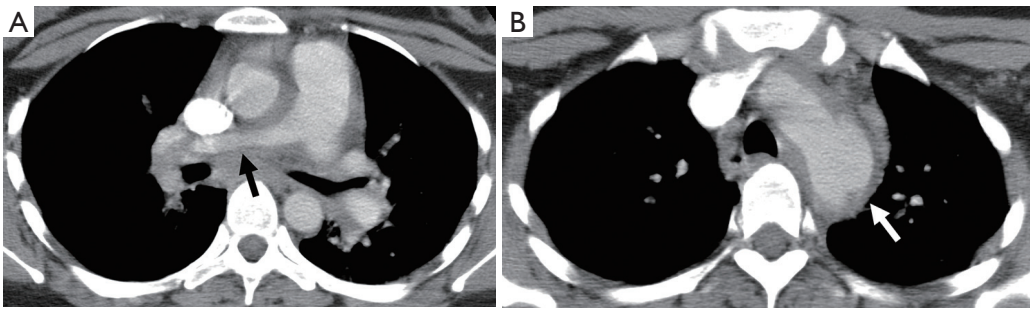

Figure 13 Takayasu arteritis. (A) Axial CT demonstrates thickening and narrowing of the right pulmonary artery (arrow). (B) Axial CT demonstrates thickening of the aorta and a focal aneurysm of the aortic arch (arrow).

young population, as it avoids radiation. Findings on MRI includes smooth wall thickening of the involved vessels, which may show enhancement. The presence of mural enhancement is suggestive of active disease. FDG-PET can show FDG uptake in acutely inflamed vessels, and also has a role to play in monitoring treatment response in these patients as the intensity of FDG accumulation decreases in response to treatment.

GCA

GCA is the most common vasculitis involving large and medium-sized arteries. It almost exclusively affects patients over 50 years of age. It predominantly affects the extracranial carotid branches and the aorta, and rarely affects the central pulmonary arteries. Pulmonary artery involvement is much less common with GCA than with Takayasu arteritis. The CT and MRI findings of GCA are similar to that of Takayasu arteritis, with evidence of arterial wall thickening, stenosis, and aneurysm (81).

Behçet disease

Behçet disease is a chronic multisystem vasculitis, which can involve large, medium, and small vessels of both the arterial and venous circulation. It usually manifests in the 2nd or 3rd decay of life. The reported prevalence of thoracic involvement of Behçet disease is up to 8%.

Behçet disease is the most common cause of pulmonary artery aneurysm, due to inflammation of the vasa vasorum of the tunica media with destruction of the elastic fibers, and resultant dilatation of the vessel lumen (79). The aneurysms in Behçet disease commonly are multiple and bilateral, and located in the lower lobe or main pulmonary arteries (82,83). They are frequently partially or totally thrombosed. CT findings also include thickening of the wall of the aorta or superior vena cava, SVC obstruction, thromboembolism, and pulmonary infarction.

Pulmonary artery aneurysm and pseudoaneurysm

Pulmonary artery aneurysms and pseudoaneurysms, whether congenital or acquired, are rare, but important to recognize because of the associated mortality. An aneurysm is a focal dilatation of a blood vessel that involves all three layers, whereas, a pseudoaneurysm does not involve all the layers of the arterial wall and is therefore at a higher risk of rupture (84). They may occur in association with a congenital cardiovascular anomaly, especially a patent ductus arteriosus; infection; neoplasm; vascular abnormality, including vasculitis, cystic medial necrosis, Marfan syndrome; and trauma, often iatrogenic. Pulmonary artery pseudoaneurysms are usually solitary, except in cases caused by endocarditis or metastatic disease, and they more commonly involve the peripheral pulmonary artery branches.

Congenital causes of pulmonary artery aneurysms and pseudoaneurysms include deficiency of the vessel wall, valvular and post-valvular stenosis, and increased flow due to left to right shunts (85). Common causes of left to right shunts which result in aneurysm formation include patent ductus arteriosus, atrial or ventricular septal defect, and sequelae of congenital heart disease repair. The risk of rupture or dissection is highest in patients with severe pulmonary hypertension associated with Eisenmenger's complex.

Pseudoaneurysms, and less commonly aneurysms, can be caused by infection with tuberculosis, pyogenic bacteria or fungi. The pseudoaneurysms associated with tuberculosis or pneumonia share a similar pathogenesis in which destruction of the vessel wall is from outer wall to inner lumen (86), and therefore occur adjacent to areas of cavitation or

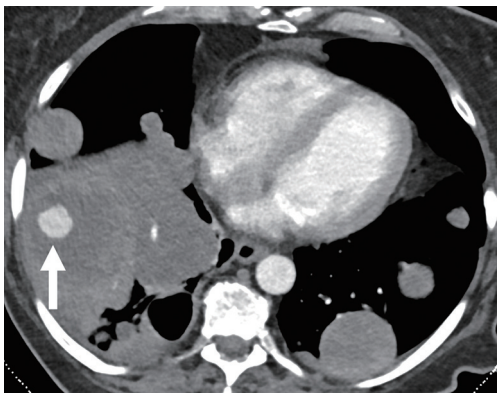

Figure 14 Pulmonary artery pseudoaneurysm due to tumor. Axial CT demonstrates bilateral pulmonary nodules and masses. Within one of the masses in the right lower lobe there is a nodular area of enhancement consistent with a pseudoaneurysm (arrow).

consolidation. Endovascular seeding of the pulmonary artery lumen by septic emboli is the proposed mechanism of mycotic pseudoaneurysm formation associated with endocarditis. In these cases, the destruction of the vessel wall starts in the lumen and progresses to the outer wall. Pseudoaneurysms secondary to endocarditis, therefore, are not necessarily related to the lung consolidation.

Primary lung cancer, and pulmonary metastases, have been reported to invade and erode into the pulmonary arteries resulting in formation of pseudoaneurysms (*Figure 14*). These most often occur where tumor nodules or masses encase the pulmonary arteries. In rare cases, primary tumors arising from the primary arteries such as leiomyosarcoma and angiosarcoma, can cause focal expansion and aneurysmal dilatation.

The most common forms of vasculitis associated with pulmonary artery aneurysms are Behçet disease (as described above) and Hughes-Stovin syndrome. Hughes-Stovin syndrome is a rare clinical disorder characterized by thrombophlebitis and multiple pulmonary and/or bronchial aneurysms (87) (*Figure 15*). Some investigators have suggested that Behçet disease and Hughes-Stovin syndrome are part of the same disease process (88).

Another major cause of pseudoaneurysm is direct injury to the pulmonary vasculature, either traumatic or iatrogenic (86). One prospective study reported a 0.2% incidence of rupture and hemorrhage after Swan-Ganz catheter insertion (89). It usually occurs when the Swan-Ganz catheter has been inserted too far, and the tip of the catheter begins to erode the wall of the vessel causing weakening and dilatation (*Figure 16*). Other iatrogenic causes include conventional angiography, chest tube insertion, biopsy, radiofrequency ablation, or surgical resection. Penetrating trauma can also cause pseudoaneurysm formation.

A high index of suspicion and awareness of the imaging findings of aneurysms and pseudoaneurysms are required to make the diagnosis. Endovascular treatment by direct coil embolization, stent placement or embolization of the feeding vessel is considered the treatment of choice.

Pulmonary arteriovenous malformations (PAVM)

PAVM are abnormal direct communications between pulmonary arteries and pulmonary veins without an intervening capillary bed. The resultant anatomic right-to-left shunts allows systemic blood to bypass gas exchange and pulmonary capillary bed processing. Clinical manifestations include asymptomatic hypoxemia, dyspnea, hemorrhage, or paradoxical emboli causing stroke, cerebral abscess or myocardial infarction. PAVM hemorrhage can be fatal, although this is a relatively rare feature except in pregnancy. As many as 90% of patients with a PAVM will prove to have hereditary hemorrhagic telangiectasia (HHT) (90). Conversely, PAVMs are present in up to 50% of patients with HHT (91-94). HHT-PAVMS are often multiple, bilateral and preferentially located at the lung bases, which is contrary to sporadic cases.

A PAVM consists of three different anatomical components: one or more feeding vessels, an aneurismal part which may be a sac or a serpiginous network, and one or more draining veins. A simple PAVM, which accounts for approximately 80% of cases, is characterized by one or more afferent feeding vessels originating from a single segmental pulmonary artery. A complex PAVM has multiple afferent feeding arteries originating from several segmental arteries.

Transthoracic contrast echocardiography is the initial screening study for PAVM in patients with HHT or high risk of HHT. For this study agitated saline is injected during echocardiography and a right-to-left shunt is diagnosed if bubbles appear in the left atrium at least four beats after their presence in the right atrium. Earlier detection of bubbles in the left atrium may be due to a patent foramen ovale and other intracardiac causes of right-to-left shunting. A positive contrast echocardiogram is followed by CT, whereas a negative study effectively excludes PAVM (95). Although the guidelines for the diagnosis and management of HHT state that unenhanced CT should follow a positive

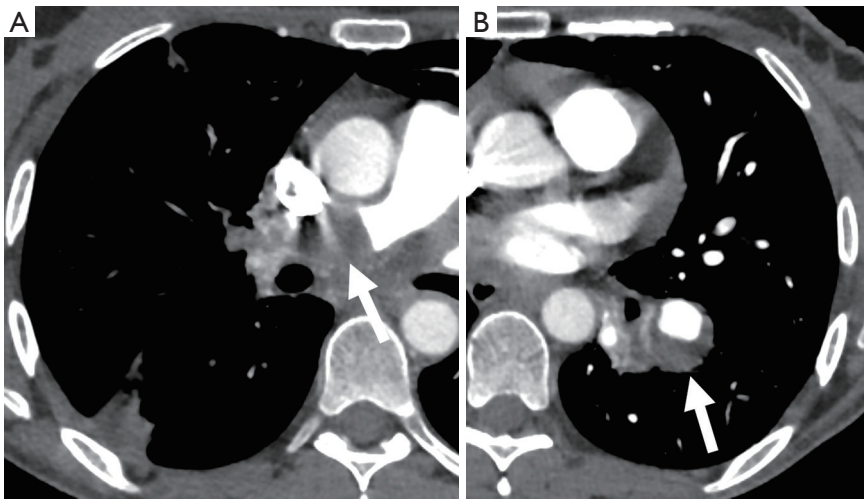

Figure 15 Hughes-Stovin syndrome. (A) Axial CT demonstrates complete occlusion of the right main pulmonary artery (arrow). (B) Axial CT shows a fusiform aneurysm with peripheral thrombus in the left lower lobe pulmonary artery (arrow).

contrast echocardiogram (91), others believe that contrast-enhanced CT provides additional information. CT, with or without contrast, allows characterization of the PAVM.

Another test which can be used in the diagnosis of PAVM and the presence of a right-to-left shunt is a nuclear lung perfusion scan. For this study macroaggregated albumin (MAA) tagged to Tc-99m is injected via a peripheral vein. In patients without a shunt, the particles are filtered by pulmonary capillaries. However, in the presence of a PAVM, a significant proportion of the particles escape into the systemic circulation and are diverted to highly vascular systemic end organ capillaries such as brain, kidney, and spleen. To estimate the right-to-left shunt in PAVM, whole body planar acquisition is performed soon after the injection of Tc-99m MAA. The amount of extra-pulmonary uptake of the tracer is directly proportional to the magnitude of the shunt (96). Tc-99m MAA perfusion scan is also useful in the evaluation of treatment response after embolization or surgical resection (97).

The classic finding of PAVM on chest radiograph is a sharply defined, round or oval nodule or mass, most commonly in the lower lobes (*Figure 17*). Feeding vessels can sometimes be seen on chest radiograph. CT is often the diagnostic imaging modality of choice. On non-contrast CT, a PAVM is a homogenous, well-circumscribed, nodule or a serpiginous mass connected with blood vessels (98). Occasionally associated phleboliths may be seen as calcifications. On contrast-enhanced CT the feeding artery, the aneurysmal part, and the draining vein enhance. 3D images are helpful delineating the anatomy, especially in cases with more than one feeding vessel. Contrast-enhanced magnetic resonance angiography is not currently performed for PAVMs screening or follow-up; however, this may change as recent studies have concluded that MRA was a contributive adjunct to pre-embolization planning (99-101), and has the advantage of no exposure to ionizing radiation

Embolization is recommended for first-line treatment of PAVMs amenable to treatment (90,102). Current guidelines recommend postembolization CT scans at 6 to 12 months, then every 3 years thereafter, and CT scans every 1 to 5 years for other patients with CT-evident PAVMs or positive contrast echocardiography studies (91). However, these have not been universally adopted due to radiation concerns.

Congenital abnormalities of the pulmonary arteries in adults

Congenital anomalies in adults may be diagnosed in symptomatic patients or found incidentally on imaging performed for other reasons.

Proximal interruption of the right or left pulmonary artery is characterized by abnormal termination of a pulmonary artery at the level of the hilum (103). The right pulmonary artery is more commonly affected and is usually an isolated finding. Whereas, interruption of the left pulmonary artery is frequently associated with congenital cardiac defects (104). The blood supply to the affected lung

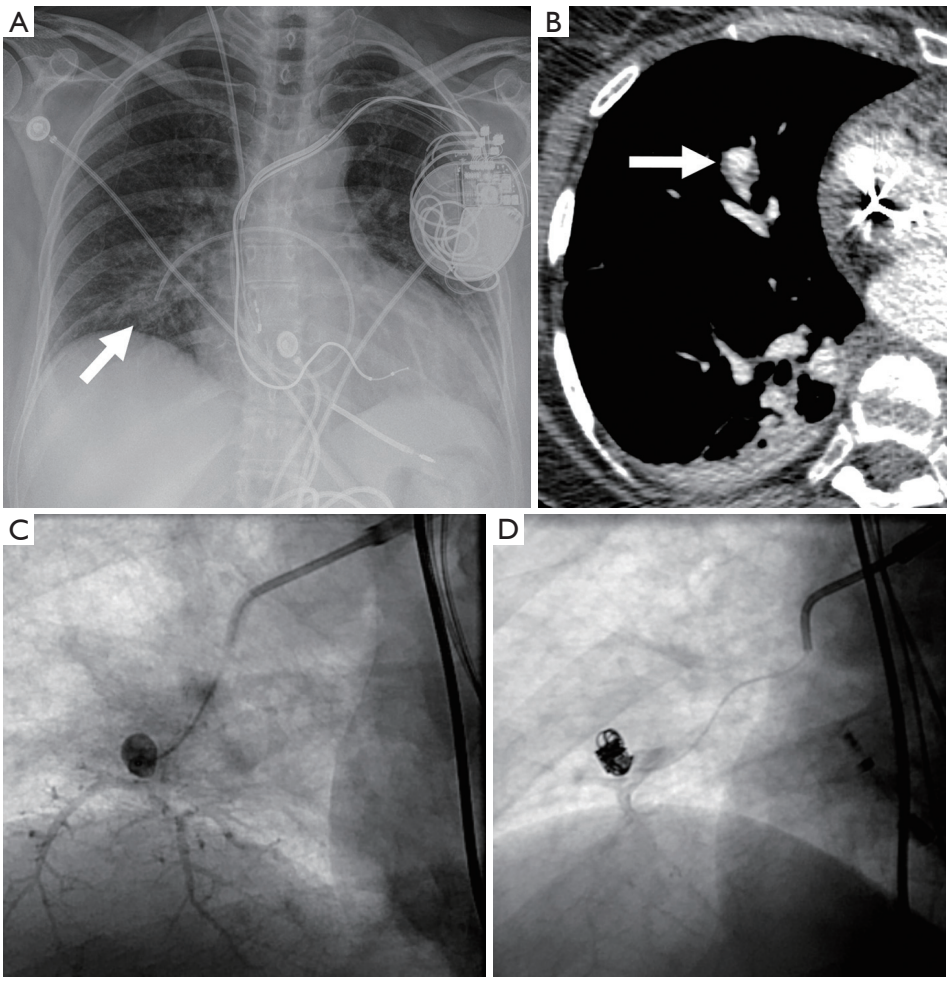

Figure 16 Iatrogenic pulmonary artery pseudoaneurysm. (A) Frontal chest radiograph demonstrates a Swan-Ganz catheter, the tip of which is inserted too far. There is an opacity adjacent to the tip (arrow). (B) Axial CT shows a pseudoaneurysm of a right middle lobe segmental artery (arrow). (C) The pseudoaneurysm was confirmed on conventional angiography. (D) This was successfully coiled.

may come from the bronchial arteries, coronary arteries, intercostal arteries or directly from the descending aorta (104-107). Although patients may be asymptomatic, most develop symptoms including dyspnea, recurrent respiratory infections, and hemoptysis (108). Ipsilateral volume loss with hyperinflation of the contralateral lung is seen on chest radiograph. Rib notching may be seen if branches of the intercostal arteries serve as collateral vessels. On CT the abnormal vessel may be completely absent or end within 1 cm of its origin (109). CT can also delineate the network of collateral arteries that supply the lung. Transpleural collaterals present as pleural thickening and subpleural parenchymal bands (110). MRI can also be used to characterize the vascular anatomy and to identify associated congenital cardiac anomalies.

Anomalous origin of the left pulmonary artery, also known as pulmonary sling, is a rare abnormality in which the left pulmonary artery arises from the posterior aspect of the right pulmonary artery and passes between the trachea and esophagus toward to the left hilum, thus forming a sling around the trachea and right main bronchus (110). Patients with pulmonary sling may have a normal tracheobronchial tree, or may have associated tracheobronchial anomalies, such as complete cartilaginous rings, or cardiovascular anomalies. The sling around the distal trachea and right main bronchus can cause compression of these structures and may lead to stenosis. The amount of stenosis correlates with the severity of the patient's symptoms including

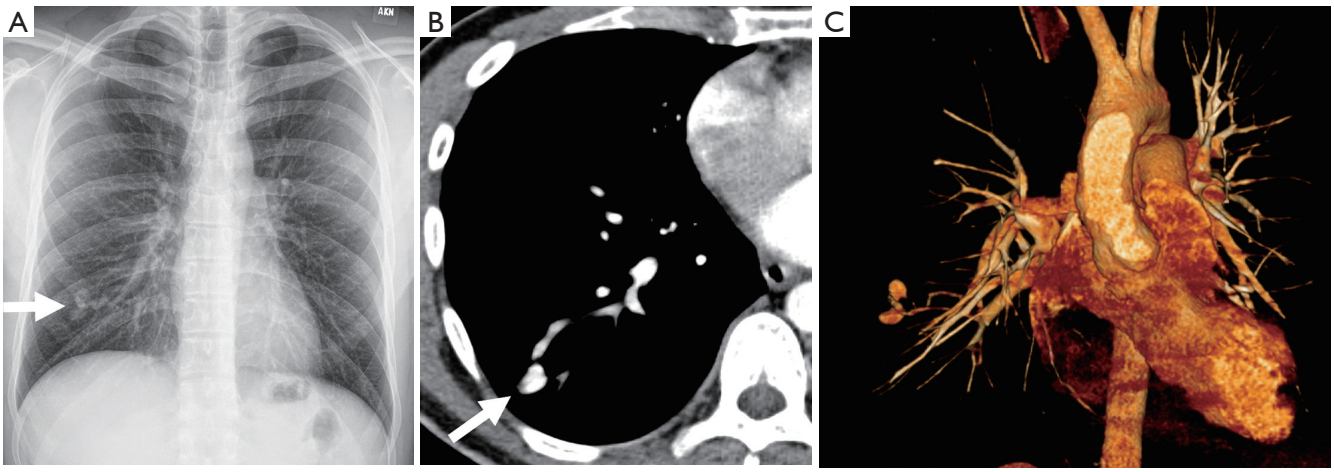

Figure 17 Pulmonary arteriovenous malformation. (A) Frontal chest radiograph demonstrates a well-defined, lobulated nodule in the right lower lung (arrow). (B) Axial contrast-enhanced CT confirms a PAVM in the right lower lobe (arrow). (C) 3D reconstruction delineates the anatomy of the PAVM. PAVM, pulmonary arteriovenous malformations.

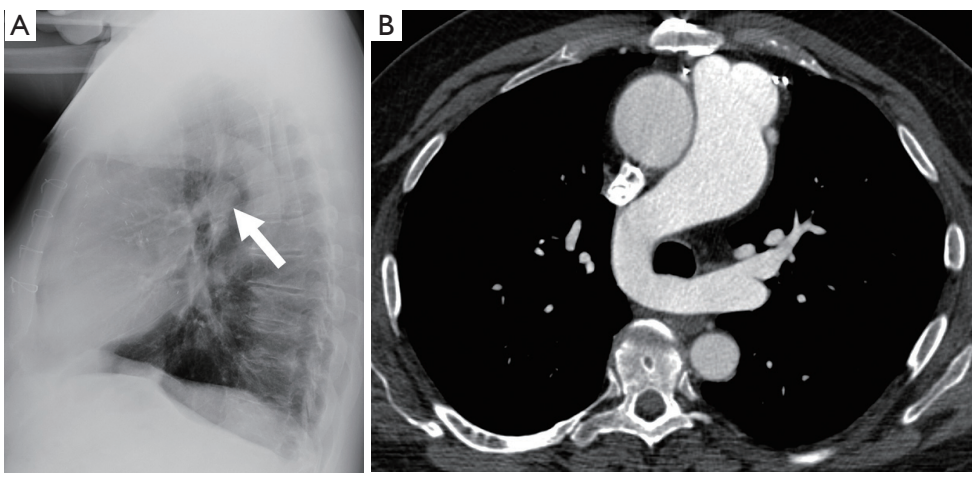

Figure 18 Pulmonary sling. (A) Lateral chest radiograph demonstrates a rounded opacity between the trachea and esophagus (arrow). (B) Axial CT shows the abnormal origin of the left pulmonary artery from the posterior aspect of the right pulmonary artery, which then passes between the trachea and the esophagus.

stridor, wheezing, and recurrent respiratory infections. A characteristic finding on a lateral chest radiograph is a rounded opacity located between the trachea and esophagus (*Figure 18*). CT reliably shows the abnormal origin and course of the artery (*Figure 18*), and allows evaluation of the airway for complete tracheal rings and tracheal stenosis. MRI can also be used to evaluate the vascular anatomy.

Idiopathic dilatation of the pulmonary trunk is another rare congenital anomaly that is characterized by abnormal enlargement of the pulmonary trunk with or without enlargement of the right and left pulmonary arteries (110). It is largely a diagnosis of exclusion after other pulmonary and cardiac causes of an enlarged pulmonary trunk have been ruled out. On chest radiograph, enlargement of the main pulmonary artery manifests as an abnormal convex contour of the left aspect of the mediastinum. On CT enlargement of the pulmonary artery greater than 29 mm can be seen.

Pulmonary artery stenosis is congenital in 95% of cases. It can be classified as valvular, which accounts for 90% of cases, subvalvular or supravalvular. Fusion of the valve

leaflets at the commissures results in restricted opening of the leaflets during systole (111). Symptoms depend on the degree of stenosis and range from an asymptomatic patient to one with signs and symptoms of systemic venous congestion mimicking congestive heart failure. Enlargement of the pulmonary trunk and left pulmonary artery, representing poststenotic dilatation, can be seen on both chest radiograph and CT. Thickened and immobile pulmonic valve leaflets, and RV enlargement may also be seen on CT. MRI is useful in evaluating pulmonic valve morphology, and can identify additional morphological abnormalities such as bulging of the pulmonic valve, reduced valve movement, and RV hypertrophy and thickening (112).

Conclusions

Many different entities, both acquired and congenital, can affect the pulmonary arteries. Radiologists need to be familiar with the indications for, and the advantages and disadvantages of the different available imaging modalities; and the imaging features of the different entities that can affect the pulmonary arteries to avoid misinterpretation and to reach the correct diagnosis.

Acknowledgments

None.

Footnote

Conflicts of Interest: The authors have no conflicts of interest to declare.

References

1. Remy-Jardin M, Remy J, Wattinne L, et al. Central pulmonary thromboembolism: diagnosis with spiral volumetric CT with the single-breath-hold technique--comparison with pulmonary angiography. Radiology 1992;185:381-7.
2. Bae KT, Tao C, Gurel S, et al. Effect of patient weight and scanning duration on contrast enhancement during pulmonary multidetector CT angiography. Radiology 2007;242:582-9.
3. Ramos-Duran LR, Kalafut JF, Hanley M, et al. Current contrast media delivery strategies for cardiac and pulmonary multidetector-row computed tomography angiography. J Thorac Imaging 2010;25:270-7.
4. Khadir MM, Chaturvedi A, Nguyen MS, et al. Looking beyond the thrombus: essentials of pulmonary artery imaging on CT. Insights Imaging 2014;5:493-506.
5. Otrakji A, Digumarthy SR, Lo Gullo R, et al. Dual-Energy CT: Spectrum of Thoracic Abnormalities. Radiographics 2016;36:38-52.
6. Stein PD, Chenevert TL, Fowler SE, et al. Gadolinium-enhanced magnetic resonance angiography for pulmonary embolism: a multicenter prospective study (PIOPED III). Ann Intern Med 2010;152:434-43, W142-3.
7. Nael K, Michaely HJ, Kramer U, et al. Pulmonary circulation: contrast-enhanced 3.0-T MR angiography--initial results. Radiology 2006;240:858-68.
8. Ersoy H, Goldhaber SZ, Cai T, et al. Time-resolved MR angiography: a primary screening examination of patients with suspected pulmonary embolism and contraindications to administration of iodinated contrast material. AJR Am J Roentgenol 2007;188:1246-54.
9. Ley S, Kauczor HU. MR imaging/magnetic resonance angiography of the pulmonary arteries and pulmonary thromboembolic disease. Magn Reson Imaging Clin N Am 2008;16:263-73, ix.
10. Kluge A, Luboldt W, Bachmann G. Acute pulmonary embolism to the subsegmental level: diagnostic accuracy of three MRI techniques compared with 16-MDCT. AJR Am J Roentgenol 2006;187:W7-14.
11. Suga K, Ogasawara N, Okada M, et al. Lung perfusion impairments in pulmonary embolic and airway obstruction with noncontrast MR imaging. J Appl Physiol (1985) 2002;92:2439-51.
12. Altes TA, Mai VM, Munger TM, et al. Pulmonary embolism: comprehensive evaluation with MR ventilation and perfusion scanning with hyperpolarized helium-3, arterial spin tagging, and contrast-enhanced MRA. J Vasc Interv Radiol 2005;16:999-1005.
13. Moody AR, Liddicoat A, Krarup K. Magnetic resonance pulmonary angiography and direct imaging of embolus for the detection of pulmonary emboli. Invest Radiol 1997;32:431-40.
14. Spuentrup E, Botnar RM, Wiethoff AJ, et al. MR imaging of thrombi using EP-2104R, a fibrin-specific contrast agent: initial results in patients. Eur Radiol 2008;18:1995-2005.
15. Kreitner KF, Ley S, Kauczor HU, et al. Chronic thromboembolic pulmonary hypertension: pre- and postoperative assessment with breath-hold MR imaging techniques. Radiology 2004;232:535-43.
16. Roeleveld RJ, Marcus JT, Faes TJ, et al. Interventricular

septal configuration at mr imaging and pulmonary arterial pressure in pulmonary hypertension. Radiology 2005;234:710-7.
17. Klok FA, Romeih S, Westenberg JJ, et al. Pulmonary flow profile and distensibility following acute pulmonary embolism. J Cardiovasc Magn Reson 2011;13:14.
18. Kavanagh PV, Stevenson AW, Chen MY, et al. Nonneoplastic diseases in the chest showing increased activity on FDG PET. AJR Am J Roentgenol 2004;183:1133-41.
19. Goldhaber SZ, Bounameaux H. Pulmonary embolism and deep vein thrombosis. Lancet 2012;379:1835-46.
20. Tapson VF. Acute pulmonary embolism. N Engl J Med 2008;358:1037-52.
21. Douma RA, Gibson NS, Gerdes VE, et al. Validity and clinical utility of the simplified Wells rule for assessing clinical probability for the exclusion of pulmonary embolism. Thromb Haemost 2009;101:197-200.
22. Klok FA, Mos IC, Nijkeuter M, et al. Simplification of the revised Geneva score for assessing clinical probability of pulmonary embolism. Arch Intern Med 2008;168:2131-6.
23. Kline JA, Mitchell AM, Kabrhel C, et al. Clinical criteria to prevent unnecessary diagnostic testing in emergency department patients with suspected pulmonary embolism. J Thromb Haemost 2004;2:1247-55.
24. Raja AS, Greenberg JO, Qaseem A, et al. Evaluation of Patients With Suspected Acute Pulmonary Embolism: Best Practice Advice From the Clinical Guidelines Committee of the American College of Physicians. Ann Intern Med 2015;163:701-11.
25. Konstantinides S. Clinical practice. Acute pulmonary embolism. N Engl J Med 2008;359:2804-13.
26. Drescher FS, Chandrika S, Weir ID, et al. Effectiveness and acceptability of a computerized decision support system using modified Wells criteria for evaluation of suspected pulmonary embolism. Ann Emerg Med 2011;57:613-21.
27. Stein PD, Fowler SE, Goodman LR, et al. Multidetector computed tomography for acute pulmonary embolism. N Engl J Med 2006;354:2317-27.
28. Worsley DF, Alavi A, Aronchick JM, et al. Chest radiographic findings in patients with acute pulmonary embolism: observations from the PIOPED Study. Radiology 1993;189:133-6.
29. Gottschalk A, Sostman HD, Coleman RE, et al. Ventilation-perfusion scintigraphy in the PIOPED study. Part II. Evaluation of the scintigraphic criteria and interpretations. J Nucl Med 1993;34:1119-26.
30. Sostman HD, Miniati M, Gottschalk A, et al. Sensitivity and specificity of perfusion scintigraphy combined with chest radiography for acute pulmonary embolism in PIOPED II. J Nucl Med 2008;49:1741-8.
31. Wittram C, Maher MM, Yoo AJ, et al. CT angiography of pulmonary embolism: diagnostic criteria and causes of misdiagnosis. Radiographics 2004;24:1219-38.
32. Kuzo RS, Goodman LR. CT evaluation of pulmonary embolism: technique and interpretation. AJR Am J Roentgenol 1997;169:959-65.
33. Hutchinson BD, Navin P, Marom EM, et al. Overdiagnosis of Pulmonary Embolism by Pulmonary CT Angiography. AJR Am J Roentgenol 2015;205:271-7.
34. Greaves SM, Hart EM, Brown K, et al. Pulmonary thromboembolism: spectrum of findings on CT. AJR Am J Roentgenol 1995;165:1359-63.
35. Casullo J, Semionov A. Reversed halo sign in acute pulmonary embolism and infarction. Acta Radiol 2013;54:505-10.
36. Marchiori E, Menna Barreto M, Pereira Freitas HM, et al. Morphological characteristics of the reversed halo sign that may strongly suggest pulmonary infarction. Clin Radiol 2018;73:503.e7-13.
37. Apfaltrer P, Sudarski S, Schneider D, et al. Value of monoenergetic low-kV dual energy CT datasets for improved image quality of CT pulmonary angiography. Eur J Radiol 2014;83:322-8.
38. Delesalle MA, Pontana F, Duhamel A, et al. Spectral optimization of chest CT angiography with reduced iodine load: experience in 80 patients evaluated with dual-source, dual-energy CT. Radiology 2013;267:256-66.
39. Kumamaru KK, Saboo SS, Aghayev A, et al. CT pulmonary angiography-based scoring system to predict the prognosis of acute pulmonary embolism. J Cardiovasc Comput Tomogr 2016;10:473-9.
40. Quiroz R, Kucher N, Schoepf UJ, et al. Right ventricular enlargement on chest computed tomography: prognostic role in acute pulmonary embolism. Circulation 2004;109:2401-4.
41. Shams A, Hung J, Bahl A. Ability of computed tomography to predict right heart strain on an echocardiogram in patients with acute pulmonary embolus. J Biol Regul Homeost Agents 2018;32:365-70.
42. Schoepf UJ, Kucher N, Kipfmueller F, et al. Right ventricular enlargement on chest computed tomography: a predictor of early death in acute pulmonary embolism. Circulation 2004;110:3276-80.
43. Wittenberg R, van Vliet JW, Ghaye B, et al. Comparison

of automated 4-chamber cardiac views versus axial views for measuring right ventricular enlargement in patients with suspected pulmonary embolism. Eur J Radiol 2012;81:218-22.
44. Stein PD, Matta F, Yaekoub AY, et al. Reconstructed 4-chamber views compared with axial imaging for assessment of right ventricular enlargement on CT pulmonary angiograms. J Thromb Thrombolysis 2009;28:342-7.
45. Lu MT, Demehri S, Cai T, et al. Axial and reformatted four-chamber right ventricle-to-left ventricle diameter ratios on pulmonary CT angiography as predictors of death after acute pulmonary embolism. AJR Am J Roentgenol 2012;198:1353-60.
46. Meinel FG, Nance JW Jr, Schoepf UJ, et al. Predictive Value of Computed Tomography in Acute Pulmonary Embolism: Systematic Review and Meta-analysis. Am J Med 2015;128:747-59.e2.
47. Takahashi EA, Reisenauer CJ, Stockland AH, et al. Pulmonary embolism attenuation is a potential imaging biomarker for pulmonary artery hemodynamic improvement after catheter-directed thrombolysis. Vasc Med 2018;23:134-8.
48. Bach AG, Taute BM, Surov A. Time to threshold as a new indicator of circulatory state and prognosis in patients with pulmonary embolism. Thromb Res 2018;161:26-32.
49. Thieme SF, Ashoori N, Bamberg F, et al. Severity assessment of pulmonary embolism using dual energy CT - correlation of a pulmonary perfusion defect score with clinical and morphological parameters of blood oxygenation and right ventricular failure. Eur Radiol 2012;22:269-78.
50. Zhang LJ, Yang GF, Zhao YE, et al. Detection of pulmonary embolism using dual-energy computed tomography and correlation with cardiovascular measurements: a preliminary study. Acta Radiol 2009;50:892-901.
51. Chae EJ, Seo JB, Jang YM, et al. Dual-energy CT for assessment of the severity of acute pulmonary embolism: pulmonary perfusion defect score compared with CT angiographic obstruction score and right ventricular/left ventricular diameter ratio. AJR Am J Roentgenol 2010;194:604-10.
52. Apfaltrer P, Bachmann V, Meyer M, et al. Prognostic value of perfusion defect volume at dual energy CTA in patients with pulmonary embolism: correlation with CTA obstruction scores, CT parameters of right ventricular dysfunction and adverse clinical outcome. Eur J Radiol 2012;81:3592-7.
53. Vedovati MC, Becattini C, Agnelli G, et al. Multidetector CT scan for acute pulmonary embolism: embolic burden and clinical outcome. Chest 2012;142:1417-24.
54. Vedovati MC, Germini F, Agnelli G, et al. Prognostic role of embolic burden assessed at computed tomography angiography in patients with acute pulmonary embolism: systematic review and meta-analysis. J Thromb Haemost 2013;11:2092-102.
55. Auger WR, Fedullo PF, Moser KM, et al. Chronic major-vessel thromboembolic pulmonary artery obstruction: appearance at angiography. Radiology 1992;182:393-8.
56. Peterson KL, Fred HL, Alexander JK. Pulmonary arterial webs. A new angiographic sign of previous thromboembolism. N Engl J Med 1967;277:33-5.
57. Korn D, Gore I, Blenke A, et al. Pulmonary arterial bands and webs: an unrecognized manifestation of organized pulmonary emboli. Am J Pathol 1962;40:129-51.
58. Renapurkar RD, Shrikanthan S, Heresi GA, et al. Imaging in Chronic Thromboembolic Pulmonary Hypertension. J Thorac Imaging 2017;32:71-88.
59. Ley S, Kreitner KF, Morgenstern I, et al. Bronchopulmonary shunts in patients with chronic thromboembolic pulmonary hypertension: evaluation with helical CT and MR imaging. AJR Am J Roentgenol 2002;179:1209-15.
60. Remy-Jardin M, Duhamel A, Deken V, et al. Systemic collateral supply in patients with chronic thromboembolic and primary pulmonary hypertension: assessment with multi-detector row helical CT angiography. Radiology 2005;235:274-81.
61. Ussavarungsi K, Lee AS, Burger CD. Mosaic Pattern of Lung Attenuation on Chest CT in Patients with Pulmonary Hypertension. Diseases 2015;3:205-12.
62. Edwards PD, Bull RK, Coulden R. CT measurement of main pulmonary artery diameter. Br J Radiol 1998;71:1018-20.
63. Remy-Jardin M, Remy J, Louvegny S, et al. Airway changes in chronic pulmonary embolism: CT findings in 33 patients. Radiology 1997;203:355-60.
64. Bannas P, Schiebler ML, Motosugi U, et al. Pulmonary MRA: differentiation of pulmonary embolism from truncation artefact. Eur Radiol 2014;24:1942-9.
65. Biederer J, Beer M, Hirsch W, et al. MRI of the lung (2/3). Why ... when ... how? Insights Imaging 2012;3:355-71.
66. van Langevelde K, Tan M, Sramek A, et al. Magnetic resonance imaging and computed tomography developments in imaging of venous thromboembolism. J

Magn Reson Imaging 2010;32:1302-12.
67. Han D, Lee KS, Franquet T, et al. Thrombotic and nonthrombotic pulmonary arterial embolism: spectrum of imaging findings. Radiographics 2003;23:1521-39.
68. Restrepo CS, Betancourt SL, Martinez-Jimenez S, et al. Tumors of the pulmonary artery and veins. Semin Ultrasound CT MR 2012;33:580-90.
69. Blackmon SH, Rice DC, Correa AM, et al. Management of primary pulmonary artery sarcomas. Ann Thorac Surg 2009;87:977-84.
70. Pu X, Song M, Huang X, et al. Clinical and radiological features of pulmonary artery sarcoma: A report of nine cases. Clin Respir J 2018;12:1820-9.
71. Mahajan A, Rekhi B, Laskar S, et al. Primary pulmonary artery sarcoma masquerading as pulmonary thromboembolism: a rare diagnosis unveiled. Clin Sarcoma Res 2017;7:13.
72. Wang X, Ren W, Yang J. Pedunculated Pulmonary Artery Sarcoma Suggested by Transthoracic Echocardiography. Echocardiography 2016;33:647-51.
73. Batista MN, Barreto MM, Cavaguti RF, et al. Pulmonary artery sarcoma mimicking chronic pulmonary thromboembolism. Radiol Bras 2015;48:333-4.
74. Yi CA, Lee KS, Choe YH, et al. Computed tomography in pulmonary artery sarcoma: distinguishing features from pulmonary embolic disease. J Comput Assist Tomogr 2004;28:34-9.
75. Liu MX, Ma ZH, Jiang T, et al. Differential Diagnosis of Pulmonary Artery Sarcoma and Central Chronic Pulmonary Thromboembolism Using CT and MR Images. Heart Lung Circ 2018;27:819-27.
76. Liu M, Luo C, Wang Y, et al. Multiparametric MRI in differentiating pulmonary artery sarcoma and pulmonary thromboembolism: a preliminary experience. Diagn Interv Radiol 2017;23:15-21.
77. Chang S, Hur J, Im DJ, et al. Dual-energy CT-based iodine quantification for differentiating pulmonary artery sarcoma from pulmonary thromboembolism: a pilot study. Eur Radiol 2016;26:3162-70.
78. Ito K, Kubota K, Morooka M, et al. Diagnostic usefulness of 18F-FDG PET/CT in the differentiation of pulmonary artery sarcoma and pulmonary embolism. Ann Nucl Med 2009;23:671-6.
79. Castaner E, Alguersuari A, Gallardo X, et al. When to suspect pulmonary vasculitis: radiologic and clinical clues. Radiographics 2010;30:33-53.
80. Matsunaga N, Hayashi K, Sakamoto I, et al. Takayasu arteritis: protean radiologic manifestations and diagnosis. Radiographics 1997;17:579-94.
81. Marten K, Schnyder P, Schirg E, et al. Pattern-based differential diagnosis in pulmonary vasculitis using volumetric CT. AJR Am J Roentgenol 2005;184:720-33.
82. Chae EJ, Do KH, Seo JB, et al. Radiologic and clinical findings of Behcet disease: comprehensive review of multisystemic involvement. Radiographics 2008;28:e31.
83. Tunaci M, Ozkorkmaz B, Tunaci A, et al. CT findings of pulmonary artery aneurysms during treatment for Behcet's disease. AJR Am J Roentgenol 1999;172:729-33.
84. Garg S, King G, Varadi G. Pseudoaneurysm of pulmonary artery: rare complication of systemic chemotherapy. Clin Case Rep 2015;3:845-8.
85. Nguyen ET, Silva CI, Seely JM, et al. Pulmonary artery aneurysms and pseudoaneurysms in adults: findings at CT and radiography. AJR Am J Roentgenol 2007;188:W126-34.
86. Chen Y, Gilman MD, Humphrey KL, et al. Pulmonary Artery Pseudoaneurysms: Clinical Features and CT Findings. AJR Am J Roentgenol 2017;208:84-91.
87. Khalid U, Saleem T. Hughes-Stovin syndrome. Orphanet J Rare Dis 2011;6:15.
88. Erkan D, Yazici Y, Sanders A, et al. Is Hughes-Stovin syndrome Behcet's disease? Clin Exp Rheumatol 2004;22:S64-8.
89. Boyd KD, Thomas SJ, Gold J, et al. A prospective study of complications of pulmonary artery catheterizations in 500 consecutive patients. Chest 1983;84:245-9.
90. Trerotola SO, Pyeritz RE. PAVM embolization: an update. AJR Am J Roentgenol 2010;195:837-45.
91. Faughnan ME, Palda VA, Garcia-Tsao G, et al. International guidelines for the diagnosis and management of hereditary haemorrhagic telangiectasia. J Med Genet 2011;48:73-87.
92. Vase P, Holm M, Arendrup H. Pulmonary arteriovenous fistulas in hereditary hemorrhagic telangiectasia. Acta Med Scand 1985;218:105-9.
93. Kjeldsen AD, Oxhoj H, Andersen PE, et al. Prevalence of pulmonary arteriovenous malformations (PAVMs) and occurrence of neurological symptoms in patients with hereditary haemorrhagic telangiectasia (HHT). J Intern Med 2000;248:255-62.
94. Haitjema T, Disch F, Overtoom TT, et al. Screening family members of patients with hereditary hemorrhagic telangiectasia. Am J Med 1995;99:519-24.
95. Zukotynski K, Chan RP, Chow CM, et al. Contrast echocardiography grading predicts pulmonary arteriovenous malformations on CT. Chest 2007;132:18-23.
96. Chokkappan K, Kannivelu A, Srinivasan S, et al. Review

of diagnostic uses of shunt fraction quantification with technetium-99m macroaggregated albumin perfusion scan as illustrated by a case of Osler-Weber-Rendu syndrome. Ann Thorac Med 2016;11:155-60.
97. Ones T, Dede F, Erdim R, et al. Quantitative shunt imaging in the evaluation of therapeutic surgery in a patient with pulmonary arteriovenous malformation. Ann Thorac Surg 2008;86:649-51.
98. Remy J, Remy-Jardin M, Wattinne L, et al. Pulmonary arteriovenous malformations: evaluation with CT of the chest before and after treatment. Radiology 1992;182:809-16.
99. Schneider G, Uder M, Koehler M, et al. MR angiography for detection of pulmonary arteriovenous malformations in patients with hereditary hemorrhagic telangiectasia. AJR Am J Roentgenol 2008;190:892-901.
100. Rotondo A, Scialpi M, Scapati C. Pulmonary arteriovenous malformation: evaluation by MR angiography. AJR Am J Roentgenol 1997;168:847-9.
101. Maki DD, Siegelman ES, Roberts DA, et al. Pulmonary arteriovenous malformations: three-dimensional gadolinium-enhanced MR angiography-initial experience. Radiology 2001;219:243-6.
102. Lacombe P, Lacout A, Marcy PY, et al. Diagnosis and treatment of pulmonary arteriovenous malformations in hereditary hemorrhagic telangiectasia: An overview. Diagn Interv Imaging 2013;94:835-48.
103. Kieffer SA, Amplatz K, Anderson RC, et al. Proximal interruption of a pulmonary artery. Am J Roentgenol Radium Ther Nucl Med 1965;95:592-7.
104. Bockeria LA, Makhachev OA, Khiriev TKh, et al. Congenital isolated unilateral absence of pulmonary artery and variants of collateral blood supply of the ipsilateral lung. Interact Cardiovasc Thorac Surg 2011;12:509-10.
105. Li X, Mu Z, Weng Z. Prenatal diagnosis of anomalous origin of pulmonary artery. Prenat Diagn 2018;38:310-7.
106. Maldjian P, Sanders AE. 22q11 Deletion Syndrome with Vascular Anomalies. J Clin Imaging Sci 2018;8:1.
107. Li Y, Zhou K, Dai J, et al. Isolated Peripheral Pulmonary Artery Hypoplasia in Adulthood Presented with Occasional Hemoptysis. Am J Respir Crit Care Med 2017;196:e52-3.
108. Bouros D, Pare P, Panagou P, et al. The varied manifestation of pulmonary artery agenesis in adulthood. Chest 1995;108:670-6.
109. Ryu DS, Spirn PW, Trotman-Dickenson B, et al. HRCT findings of proximal interruption of the right pulmonary artery. J Thorac Imaging 2004;19:171-5.
110. Castaner E, Gallardo X, Rimola J, et al. Congenital and acquired pulmonary artery anomalies in the adult: radiologic overview. Radiographics 2006;26:349-71.
111. Ryan R, Abbara S, Colen RR, et al. Cardiac valve disease: spectrum of findings on cardiac 64-MDCT. AJR Am J Roentgenol 2008;190:W294-303.
112. Didier D, Ratib O, Lerch R, et al. Detection and quantification of valvular heart disease with dynamic cardiac MR imaging. Radiographics 2000;20:1279-99; discussion 1299-301.

Cite this article as: Leitman EM, McDermott S. Pulmonary arteries: imaging of pulmonary embolism and beyond. Cardiovasc Diagn Ther 2019;9(Suppl 1):S37-S58. doi: 10.21037/cdt.2018.08.05

